Land-Use Land-Cover Classification and Its Change Detection Using Multi-Temporal Landsat Data

Shiv Raj[1], Surinder Deswal[2]*

[1,2] Department of Civil Engineering, National Institute of Technology Kurukshetra, Kurukshetra, India.
*Corresponding author

(Received: 23.08.2025; Accepted: 01.09.2025)
Web link: https://ijths.com/volume-1-issue-1-july-september-2025/

Abstract

This study discusses the effect of land-use land-cover (LULC) change on the land surface temperature in the Gaya district of Bihar (India). Landsat data acquired from 1993 to 2023 were used for land cover classification as well as land surface temperature calculation. The predominant patterns of change in land cover are characterised by an increase in agricultural land area (+4.93%), built-up areas (+1.51%), and water bodies (+2.01%), accompanied by a decline in forest cover (4.23%) and barren terrains (4.23%). The findings of this study also suggest a strong inverse correlation between land surface temperature (LST) and normalised difference vegetation index (NDVI) and a strong positive correlation with normalised differences built-up index (NDBI). The actual temperature and temperature computed from the thermal band of Landsat images exhibited a strong correlation (0.979) with a low root mean square error (1.98). The average percentage decline of 5.42% showed that the computed land surface temperature was on the higher side of the actual measured temperature. The results of the study demonstrated a significant decline in vegetation cover in the study area due to increased population leading to urbanisation and infrastructure development, thus continuously changing the ecology of the region.

Keywords: *Land-use land-cover (LULC); Land surface temperature (LST); Normalised difference vegetation index (NDVI); Normalised differences built-up index (NDBI); Kappa coefficient*

INTRODUCTION

Increased urbanisation and industrialisation, coupled with the fast change in land-use and land-cover (LULC), have been contributing to a range of environmental and ecological concerns in recent decades, particularly in developing regions (Saharan *et al.*, 2024). Several studies have documented the land-cover changes from vegetation cover to agricultural and urban land uses, as well as the conversion of agricultural land to urban areas (Ahmad *et al.*, 2017). These LULC changes have been found to have direct and indirect detrimental impacts on a range of ecosystem services that may include desertification, global warming and climate change, hydrological and bio-geochemical cycles, degradation of water resources, droughts and floods, agriculture output, wildlife, etc. (Conrad *et al.*, 2013; Gondwe *et al.*, 2021; Hashim *et al.*, 2020; Kawo *et al.*, 2021; Laosuwan and Sangpradit, 2012; Moldakhanova *et al.*, 2023; Yermekbayev *et al.*, 2023; Yussupov and Suleimenova, 2023). So, the need to study the changes in LULC through quantitative measurement is of utmost importance in determining the impact on the value of ecosystem services. The incorporation of such an approach may potentially facilitate the process of making informed decisions regarding the sustainable and enduring development of ecosystems.

Manual approaches to LULC classification and change detection present a challenge due to the requirement of resources as well as the limitations of ground-based surveying. With the free availability of medium-resolution satellite imagery, LULC classification and mapping or change detection studies covering large areas have become possible and are being used by various studies (Chaudhuri and Mishra, 2016; Hashu and Gebre-Egziabher, 2018; Koko *et al.*, 2021). The use of modern computer-based LULC approaches is not only efficient and economical but also advantageous in identifying errors on historical classification maps, which usually lack ground truth samples (Egorov *et al.*, 2018; Reis, 2008; Robertson and King, 2011; Wang *et al.*, 2017). Moreover, it provides the additional benefit of

presenting a more comprehensive elucidation of the results related to this classification (Bisht *et al.*, 2023; Kausarian *et al.*, 2023).

Keeping in view the usefulness of satellite images, the present study used Landsat-5, Landsat-7 and Landsat-8 images covering a period of 30 years from March 1993 to March 2023 for the classification of LULC in the study area or area of interest (AOI), that is Gaya district of Bihar State in India. The study aims to provide valuable insights for the effective management, planning and sustainable development of the study area /AOI to prevent the occurrence of human-induced environmental catastrophes, such as floods, droughts, urban heat island effect, weather extremities, crop yield, etc., due to rapid urbanization (Shekhar and Godihal, 2023). The main objectives of the study include –

- to analyze the impact of land-use land-cover (LULC) changes of the study area/AOI for the past three decades using remote sensing & GIS techniques;
- computation of land surface temperature (LST) and its fluctuations using Landsat-5, Landsat-7, and Landsat-8 data;
- determining the correlation between normalised difference vegetation index ($NDVI$), normalised differences built-up index ($NDBI$), and LST; and

variation of actual local temperature and satellite-computed temperature over the study area.

MATERIALS AND METHODS

Study Area

The Gaya district is the second largest district of the state of Bihar (India), having an area of 4,976 km^2 (Fig. 1). It is a highly populated region having a population density of 883 per km^2 with a high population growth rate of 26.43 % during the period of 2001-2011(Census, 2011).

The region has a strong historical agricultural background due to a humid subtropical climate with 1,062 mm average annual rainfall evenly distributed throughout the year. In the last three decades, it has emerged as a highly active region for tourism, urbanisation, and economic development. As a result, the region has undergone significant changes in land-use and land-cover (LULC).

Methodology

The methodology employed in this study includes downloading Landsat data from the USGS website and applying some pre-processing, such as mosaic and subset analysis. Fieldwork in 2023 was also carried out for ground truth data collection using on-site investigation and observation. Standard procedures were employed for the analysis of the data used in the study. The initial segment of the study encompassed the process of data preparation and collection, while the subsequent section delved into the analysis of the data.

Data Acquisition

Multi-spectral data acquired by the Landsat satellite and provided by the USGS Earth Explorer (https://earthexplorer.usgs.gov/) spanning over a 30-year period (1993-2023) were downloaded for the purpose of LULC classification, change detection, and LST calculation covering the Gaya district. Keeping in view of the cloud cover and its impact on the accuracy of LULC classification over the study area, all images having less than 10% cloud cover were used. Table 1 provides the details of the Landsat images used in this study. Pre-processing of satellite pictures is a vital stage prior to using them for LULC classification, with the purpose of creating linkages between biophysical phenomena and available data. The essential pre- and post-processing of all Landsat images was carried out using ERDAS Imagine and Arc GIS software.

Various spectral bands were integrated into one layer using layer stacking in ERDAS IMAGINE Software. Following this, a subset image covering the study area was obtained through the process of superimposing a shape file of the designated study region onto each stacked image. The maximum likelihood classifier was employed to classify the images to create an LULC map within ArcGIS. The classification of land use has been conducted by considering bands 1 to 5 and band 7 of Landsat-5 TM imagery. However, band 6 was excluded from the analysis due to its thermal nature. Conversely, the utilization of bands 1–7 has been considered for the categorization of land use with Landsat-8

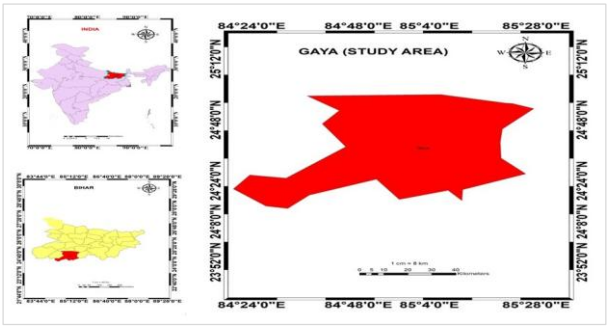

Fig. 1: Location map of the area of interest.

Table 1: Details of satellite images used in the analysis.

Satellite	Month of data acquisition	Path / row	Spatial resolution (ns)	Land cloud (%)	Scene cloud (%)	Day / night
Landsat-5 TM	March, 1993	141,43	30 m	0	0	Day
Landsat-7 ETM+	March, 2003	141,43	30 m	0	0	Day
Landsat-8 OLI	March, 2013	141,43	30 m	1	1	Day
Landsat-8 OLI	March, 2023	141,43	30 m	0	0	Day

OLI imagery. Sufficient numbers of training samples were used for the LULC classification of all four images.

Land-Cover Classification Scheme

A categorization method that details the LULC classes has been considered while developing the LULC map using Landsat photos. The optimum quantity of LULC classes to be taken depends on the objective of the study. In this study, built-up areas, forests, water bodies, agriculture, and barren land were chosen as the five most important LULC classes for mapping the whole region. The primary colours of red, green, and blue (RGB) were used to produce the FCC (False Colour Composite) of all images during the initial stage of the analysis of the stacked image, which proved to be very useful for distinguishing between various types of land cover. Here, the FCC's RGB bands 5, 4, and 3 were chosen. Using satellite imagery, thematic maps were generated that distinguish between five distinct types of land-use classes in the study area (Table 2).

Table 2: Land-use classes with their description.

LU Classes and its colour	Description
Built-up land / Urban area (Red)	Settlements, industrial areas, commercial areas, rural areas, mining
Forest cover (Green)	Deciduous, scrub forest
Water body (Blue)	Rivers, ponds and lakes
Agricultural land (Yellow)	Cropland, fallow land, plantation
Barren land (Brown)	Scrub land, sandy area, rocky area without vegetation cover

Image Classification

To generate thematic maps of different years, supervised classification with the maximum likelihood method was employed in this study. In this study, training samples ranging from 75 to 85 were collected for each land-use (LU) class. These samples were then aggregated to generate a map with LU-specific themes. Following the generation of classification results, the recoding tool was employed within the ERDAS software to effect specific modifications aimed at rectifying the misclassification of pixels.

Due to the use of pixel-based image classifications covering the study area, images are found to have salt and pepper noise. To remove this noise, post-classification processing using a 3×3 mode filter was employed within the ERDAS IMAGINE software. This process transforms individual pixels into the neighbourhood class that was most frequently observed.

Analysis

Performing change detection of time series LULC

Change detection analysis is a process that involves the measurement and quantification of the dissimilarities between images of a particular region captured at different time intervals. This form of analysis is highly beneficial in detecting alterations in LULC, including an increase in built-up land and a decline in agricultural land. The analysis calculated statistical measures for detecting changes in the data from the time intervals 1993–2003, 2003–2013, and 2013–2023. Change detection employs a range of algorithms for detecting changes, such as image differencing, image rationing, and post-classification techniques, to provide insights into alterations that have occurred within a chosen area of interest.

The present study utilised ArcGIS and MS Excel to identify changes in LULC categories. This was accomplished by generating cross-tabulations or change matrices. The change matrix facilitates comprehension of the probability of transitioning between distinct land use and land cover categories. The matrix displays LULC categories for the present year in the columns, while the rows correspond to the LULC categories for the preceding year. The matrix provides information regarding the net change, gain, and loss experienced by each land use and land cover category, along with details of the spatial distribution of these alterations. In this matrix element in central diagonal axis like one class for example Built-up area to Built-up area this area has no change means none of its pixels is converted to another class during time lapse and therefore overall area has no change because the present study has considered the same order during matrix formation.

Accuracy assessment of LULC maps

LULC accuracy is a metric that quantifies the degree of correspondence between the obtained outcomes and the actual values. The evaluation of precision is a crucial aspect in the analysis of land-use and land-cover change detection. The present investigation involved an analysis of the accuracy assessment of land use and land cover (LULC) classification through the utilisation of the confusion matrix (Boori *et al.*, 2015; Hassan *et al.*, 2016). The accuracy assessment tool of ERDAS Imagine used a comparative analysis between the initial, unprocessed satellite image and the image that was later classified. A total of 100 sampling points were chosen through a random selection process. Based on visual analysis, utilisation of Google Earth Images, and cross-referencing with ground truth data in cases of uncertainty, precise sample locations within the initial unclassified image were identified. The accuracy assessment table documented a "reference point" upon zooming in and identifying a particular location. Each image of the classified land use category was evaluated using a distinct viewer to guarantee precision, and the outcomes were documented as accurate or inaccurate based on the assigned points.

The approach used to calculate precision remains uniform throughout all discrete land utilisation classifications. Overall accuracy was computed by using Eq. 1 (Lunetta *et al.*, 2001; Pal and Ziaul, 2017; Zhou *et al.*, 1998). The comparison of classified images was conducted using two Eqs. 2 and 3, representing user and producer accuracies, respectively.

$$Overall\ Accuracy = \frac{Total\ number\ of\ correctly\ classified\ pixel\ (diagonal)}{Total\ number\ of\ reference\ pixels} \quad (1)$$

$$User\ Accuracy = \frac{Diagonal\ value\ of\ row \times 100}{Row\ total} \quad (2)$$

$$Producer\ Accuracy = \frac{Diagonal\ value\ of\ column \times 100}{Column\ total} \quad (3)$$

The Kappa coefficient (k) is calculated in the study to assess the precision of the maps. This statistical measure of agreement is used as an alternative approach to evaluating the land-use map across all four studied years. Kappa coefficient is a metric that ranges from 0 to 1 (Foody, 1992; Ma and Redmond, 1995; Pal and Ziaul, 2017). The numerical scale used in this context ranges from 0 to 1, where 0 denotes the lowest possible value and 1 denotes the highest possible value. Kappa values between 0.40 and 0.55 have been interpreted as indicating acceptable accuracy, between 0.55 and 0.70 as indicating high accuracy, between 0.70 and 0.85 as indicating very good accuracy, and beyond 0.85 as indicating unusually great accuracy. This led to the creation of LU-classified regions, error assessment matrices, and thematic maps. The quality of the generated maps is improved by accuracy evaluation, which also helps in comprehending the causes and consequences of errors. The process of assessing accuracy serves to augment the quality of a classified map and facilitate comprehension of any deficiencies and their corresponding impacts.

Surface temperature monitoring

Rising surface temperatures pose a challenge in today's society. The correlation between rising temperatures and the spread of human settlements has been evaluated by computing the land surface temperature (LST) using Landsat data. Since only the thermal band is required for the extraction of LST data, the study used Band-6 from Landsat-5 TM for 2003 and 1993 and Band 10 from Landsat-8 for 2013 and 2023. Ding and Shi (2013) outlined six steps that are necessary to obtain LST information from the Landsat thermal bands using ArcGIS.

*Spatial indices and relation with **LST***

Two indices exhibiting a relation among surface temperature, built-up area, and vegetation using LANDSAT data were computed. These indices are $NDBI$ (Normalised Differences Built-up Index) and $NDVI$ (Normalised Differences Vegetation Index). Townshend and Justice (1986) recommended Eq. 4 to be used for calculating $NDVI$, as given under:

$$NDVI = \frac{(NIR\ band - R\ band)}{(NIR\ band + R\ band)} \quad (4)$$

where NIR refers to the near-infrared spectrum and R refers to the red. The $NDVI$ was calculated using bands 3 and 4 of the Landsat TM data and bands 4 and 5 of the Landsat OLI data. The $NDVI$ measures the amount of vegetation in a given

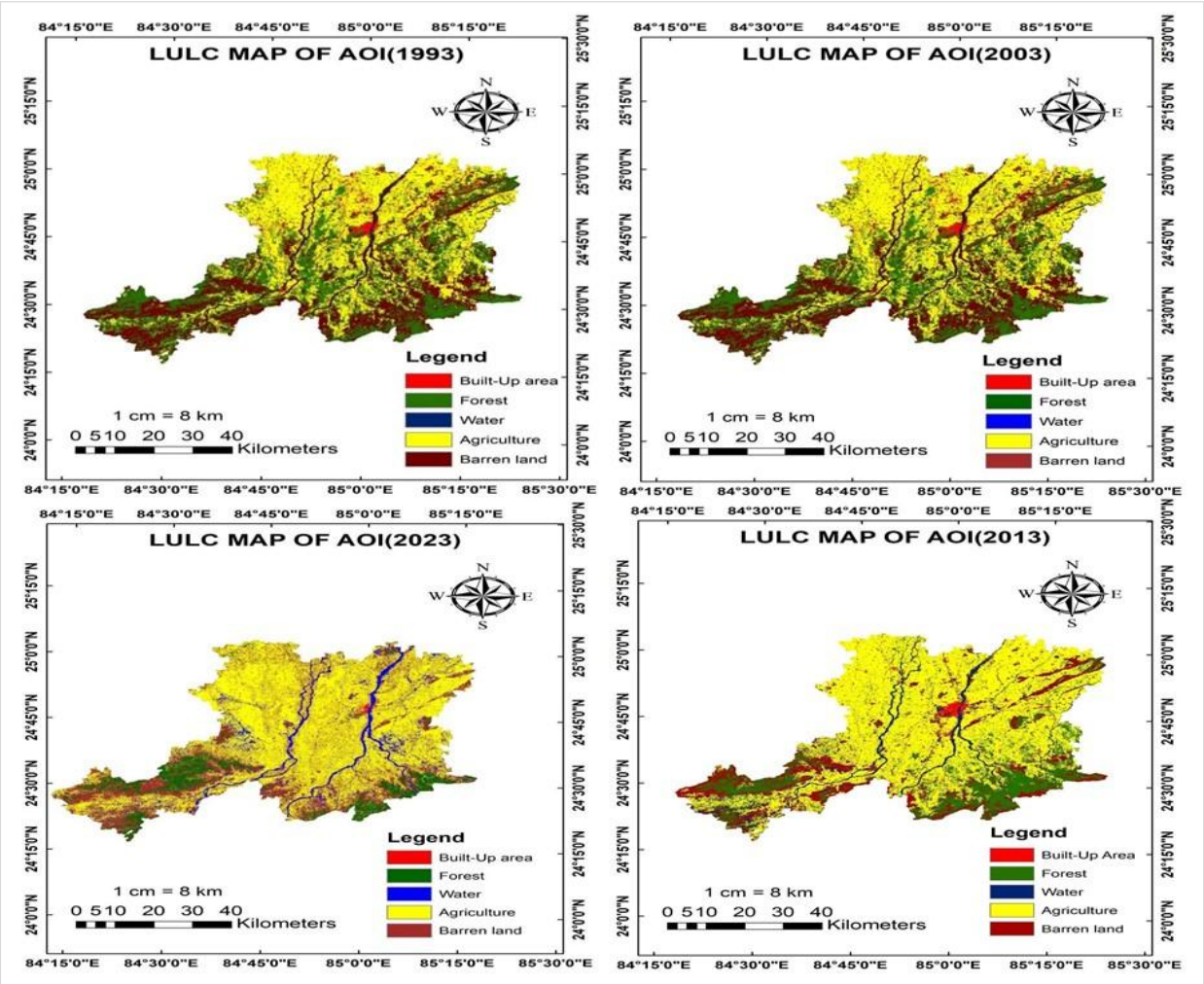

Fig. 2: LULC maps of AOI in 1993, 2003, 2013 and 2023.

region (Pranoto *et al.*, 2023). $NDVI$ values can be either minus one or plus one. Vegetation cover is represented by values between 0 and +1, with values closer to 1 indicating dense vegetation. $NDBI$ is computed using Eq. 5 given as under (Zha *et al.*, 2003):

$$NDBI = \frac{(MIR\ band - NIR\ band)}{(MIR\ band + NIR\ band)} \quad (5)$$

where MIR is the middle infrared spectral region. The $NDBI$ was calculated using Landsat TM data from bands 5 and 4 and OLI data from bands 6 and 5. The built-up index of a region is denoted by the acronym $NDBI$. It can have a value anywhere from -1 to 1. Built-up is shown by a value between 0 and +1, with a number closer to 1 indicating a high concentration of structures.

RESULTS AND DISCUSSION

Decadal LULC Description of Classified Images

Five land cover classes describe land information usage in the study area: built-up area, dense cover of trees, water bodies, crop land, and uncultivable land. Classified images obtained for the years 1993, 2003, 2013 and 2023 are shown in Fig. 2.

The LULC classification of the satellite image from 1993 (Fig. 2) indicates that the regions of water bodies and built-up land area were comparatively small, while agricultural land occupied a good portion of the area. The LULC in the eastern region is predominantly agricultural, with some areas having undergone sub-division; whereas, there is a dense forest canopy in the southern high terrain of the region.

In the year 2003, there was a significant reduction in the extent of open forest and barren land cover (Fig. 2). The findings indicated an increase in cultivable land area within the region as compared to previous records. The expansion of urban or developed areas exhibited a greater increase compared to LULC in 1993. The dense forests of the southern region have undergone a transformation, whereby a portion of the area has been replaced by an open forest. The visible in 2013 (Fig. 2). A slight increase in the total area of croplands was observed for both types of agricultural land compared to the previous year. The decreasing trend of forest cover still continues till 2013. Additionally, there were areas characterized by scrub vegetation, and the accumulation of sand was observed to have diminished.

Forest areas covered a larger portion of the study region in the years 1993, 2003, 2013, and 2023. The forested areas are known to have a significant impact on the hydrological cycle through their ability to facilitate water infiltration and mitigate the removal of the top layer of soil. The data indicate a declining pattern in the forest from 1993 to 2023. Cropland was identified as the second most prevalent land cover in the study region during the year 1993. Subsequent to 2013, a significant reduction in crop land was observed during the period spanning from 2013 to 2023. The decrease in arable land can be predominantly attributed to its reallocation for non-agricultural objectives. The data pertaining to agriculture and plantation land exhibits an upward trajectory from 1993 to 2013, followed by a decline in 2023. The data indicates a rising trend in the built-up land area between the years 1993 and 2023. The study area exhibits a positive correlation between population growth and the loss of agricultural land, as well as the rise of built-up land.

LULC Change Detection Analysis

The main patterns of change between 1993 and 2023 indicated an increase in agricultural land, developed land, and a small number of water bodies, with a decline in forested and arid areas. Between 1993 and 2023, the share of built-up land/urban area expanded from 4.03% to 5.54%, while the area of water bodies increased from 3.82% to 5.84%, and agricultural land expanded from 64.41% to 69.34% (Table 3). However, the share of forest and arid (barren) terrain decreased from 20.13% to 15.90% and from 7.61% to 3.38%, respectively. Fig. 3 shows the comparative change analysis for three decades.

Table 3: LULC change of study area during 1993 – 2023.

Area / LULC Class / Year	km^2	%	km^2	%	km^2	%	km^2	%	km^2	%
	1993		2003		2013		2023		Overall change from 1993 to 2023	
Built-up land/ Urban area	200	4.03	215	4.33	225	4.53	275	5.54	75	1.51
Forest cover	1,000	20.13	950	19.12	850	17.11	790	15.90	-210	-4.23
Water body	190	3.82	200	4.03	220	4.43	290	5.84	100	2.01
Agricultural land	3,200	64.41	3,400	68.48	3,500	70.45	3,445	69.34	245	4.93
Barren land	378	7.61	203	4.09	173	3.48	168	3.38	-210	-4.23
Total	4,968	100.00	4,968	100.00	4,968	100.00	4,968	100.00	00	00.00

expansion of cropland has resulted in a corresponding increase in agricultural land. This was possibly because of population growth, which led to the creation of more areas required for the settlement of people.

Water bodies in 2013 were observed to be comparable to 2003 (Fig. 2). The increase in urban settlement is clearly Built-up land or urban area in the region has exhibited consistent expansion from 1993 to 2023. Over a period of 30 years, the rate of urbanisation in the Gaya region was observed to be significant, with an average annual rate of increase of 2.5 km^2 in urban area. The rate of growth was more pronounced during the period 2013 to 2023 with an

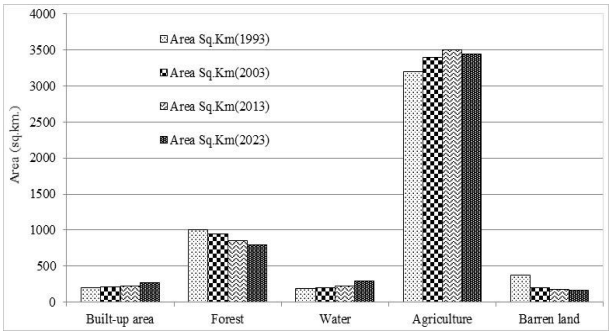

Fig. 3: Comparative changes of different classes over three decades from 1993 to 2023.

estimated annual increase of 5 km^2. The analysis of the pace of metropolitan development has revealed that there is no systematic guideline for urbanisation, but there is consistent growth in the urban area.

The area of dense forest experienced a continuous decrease from 1993 to 2023 accounting for a total decrease of 210 km^2 (-4.23%), as evidenced by the data presented in Table 3, which indicates a conversion of said area to agricultural and residential land use. During the first decade of the study period (1993–2003), a total of 50 km^2 of dense forest were removed with an annual rate of change of 5 $km^2/year$, followed by conversion of additional 100 km^2 with an annual rate of 10 km^2 during 2003-2013, and further conversion of 60 km^2 with an annual rate of 6 km^2 during 2013–2023. There has been a continual decrease in the amount of land covered by dense forests within a decade or less.

The region exhibits a consistent upward trend in the size of water bodies over the period spanning from 1993 to 2023 (Table 3). In 1993, the water body covered an area of 190 km^2; whereas, in 2003, the area had expanded to encompass a total of 200 km^2. During the period of 1993–2003, a minimal annual fluctuation was observed. The findings indicate that from 1993–2013, the area experienced a limited increase in water bodies (190-220 km^2) or 3.82-4.43% throughout the year. However, there was a noticeable increase in water body area in 2023, amounting to 290 km^2 (5.84%), which can be attributed to the increased flooding conditions on land surfaces, intensification of rainfall, and significant changes in climatic conditions over the past few decades.

Table 3 depicts a gradual increase in agricultural land area between 1993 and 2013, followed by a marginal decline in the succeeding decade, with an overall increase of 245 km^2

Table 4: Accuracy assessment and Kappa coefficient of LULC image in 1993, 2003, 2013 and 2023.

Class	Built-up land /Urban area	Forest cover	Water body	Agricultural Land	Barren land	Accuracy, in %			Kappa Coeff. (*k*)
						User	Producer	Overall	
1993									
Built-up land / urban area	10	0	0	0	0	100	100.00	88.00	0.850
Forest cover	0	10	0	0	0	100	83.33		
Water body	0	0	7	0	3	70	100.00		
Agricultural land	0	1	0	8	1	80	100.00		
Barren land	0	1	0	0	9	90	69.23		
Total Points (50)	10	10	7	8	13				
2003									
Built-up land / urban area	10	0	0	0	0	100	100.00	86.00	0.825
Forest cover	0	9	0	1	0	90	90.00		
Water body	0	0	7	0	3	70	100.00		
Agricultural land	0	0	0	9	1	100	81.81		
Barren land	0	1	0	1	8	100	66.67		
Total Points (50)	10	10	7	11	12				
2013									
Built-up land / urban area	10	0	0	0	0	100	100.00	92.00	0.900
Forest cover	0	10	0	0	0	100	100.00		
Water body	0	0	9	0	1	90	90.00		
Agricultural land	0	0	0	9	1	90	90.00		
Barren land	0	0	1	1	8	80	80.00		
Total Points (50)	10	10	10	10	10				
2023									
Built-up land / urban area	9	0	0	0	1	90	100.00	84.00	0.806
Forest cover	0	9	0	1	0	90	100.00		
Water body	0	0	7	2	1	70	87.50		
Agricultural land	0	0	0	9	1	90	69.20		
Barren land	0	0	1	1	8	80	72.72		
Total Points (50)	9	9	8	13	11				

(+4.93%) during the study period. The share of agricultural land area increased by 200 km^2 (6.25%) during 1993-2003, followed by an additional increase of 100 km^2 (2.94%) during 2003-2013, with a marginal decline of 5 km^2 (-0.14%) during 2013-2023. The presence of open or dense vegetation was observed in a significant portion of the rural area, resulting in distinct reflectance captured by satellite imagery, which depicted pixels as eroded lands. The expansion of the farming region by 300 km^2 between 1993 and 2013 can be attributed to the use of previously unused arable land for agriculture. Results also suggest a decrease in agricultural land cover from 2013-2023 due to an increase in other developmental activities.

Barren land made up 7.61% (378 km^2) of the total land in the region in 1993 that gradually decreased to 4.09% (203 km^2) in 2003, 3.48% (173 km^2) in 2013, and 3.38% (168 km^2) in 2023, thus accounting for an overall decline of 4.23% (210 km^2) during the study period (Table 3). The majority of the barren or unproductive land was used for farming or other activities. The area covered by this class underwent the most significant decline during the first 10 years of the study period (1993–2003) at the annual rate of 17.5 km^2, while the least decline at the annual rate of 0.5 km^2 was observed during 2013-2023. It's possible that rough or deserted areas quickly transformed into rural land and neighbourhoods to meet the demands of the expanding population.

Accuracy Assessment of Classes

The categorisation of LULC classes is a significant aspect of land management and analysis. The process of evaluating the accuracy of land cover classification using remote sensing images involves the creation of a confusion matrix. The Kappa coefficient (k) is also employed to ascertain statistical significance in the confusion matrix; “user accuracy” and “producer accuracy” are also computed (Table 4) of the studied years, i.e., (1993–2023).

Decadal Changes in *LST*

The impact of land use practices on the environment, both at the local and regional levels, is considered to be a crucial and prominent issue. This is because land use practices have the potential to affect not only climatic conditions but also ecosystems. The expansion of LULC regions is indicative of positive change, while a reduction in these regions represents negative change (Das *et al.*, 2021). The areas designated as forest cover and farming serve as carbon sinks. Despite their varying capacities for carbon sequestration, they exhibit certain similarities. The quantity of carbon sequestered is subject to variation across different forest types. Non-vegetated regions are known to elevate GHG (greenhouse gas) emissions and reduce carbon levels, whereas vegetated regions are capable of absorbing and retaining atmospheric carbon. The current understanding is that anthropogenic emissions of greenhouse gases have a significant impact on terrestrial ecosystems.

The practices of deforestation, insufficient agricultural land, and increasing urbanization have discernible effects on the temperature and precipitation patterns at the local and regional levels. The current situation has the potential to alter the global albedo, which refers to the ratio of diffuse reflectivity or the ability of the Earth's surface to reflect solar

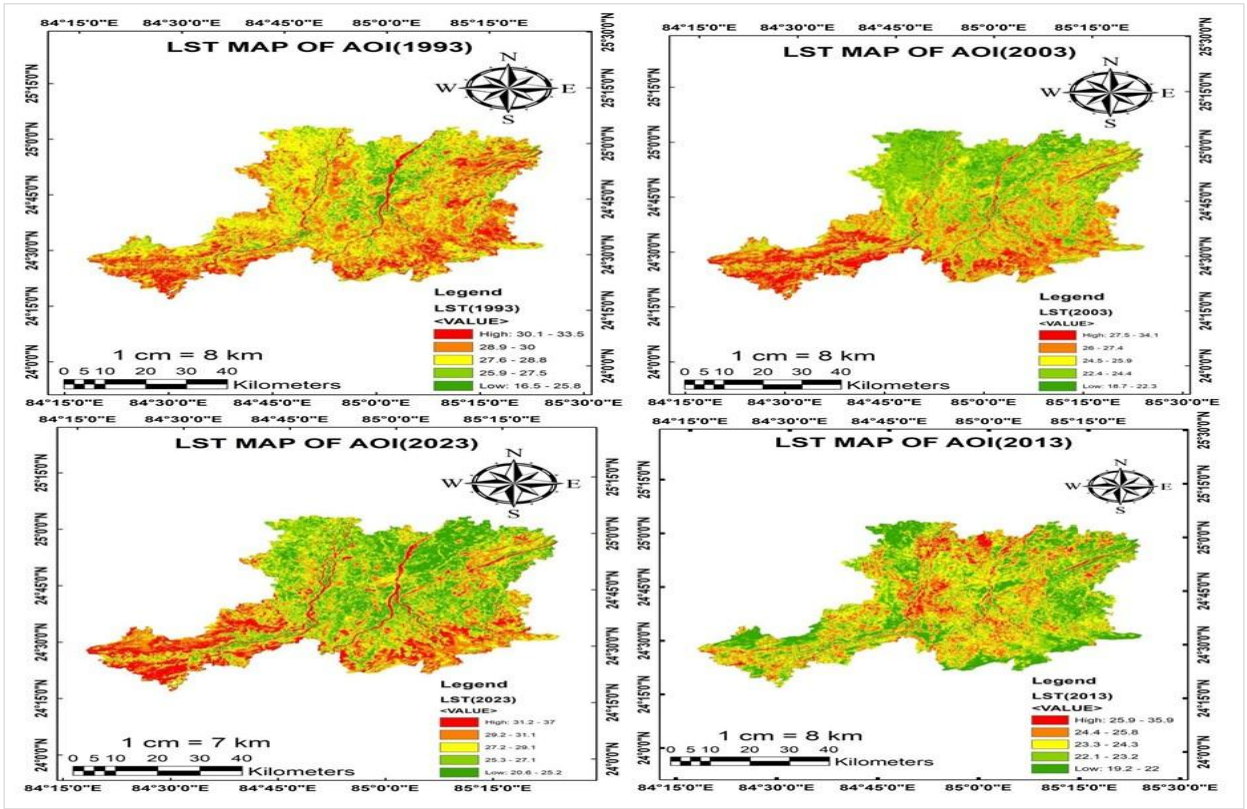

Fig. 4: *LST* maps of AOI in 1993, 2003, 2013 and 2023.

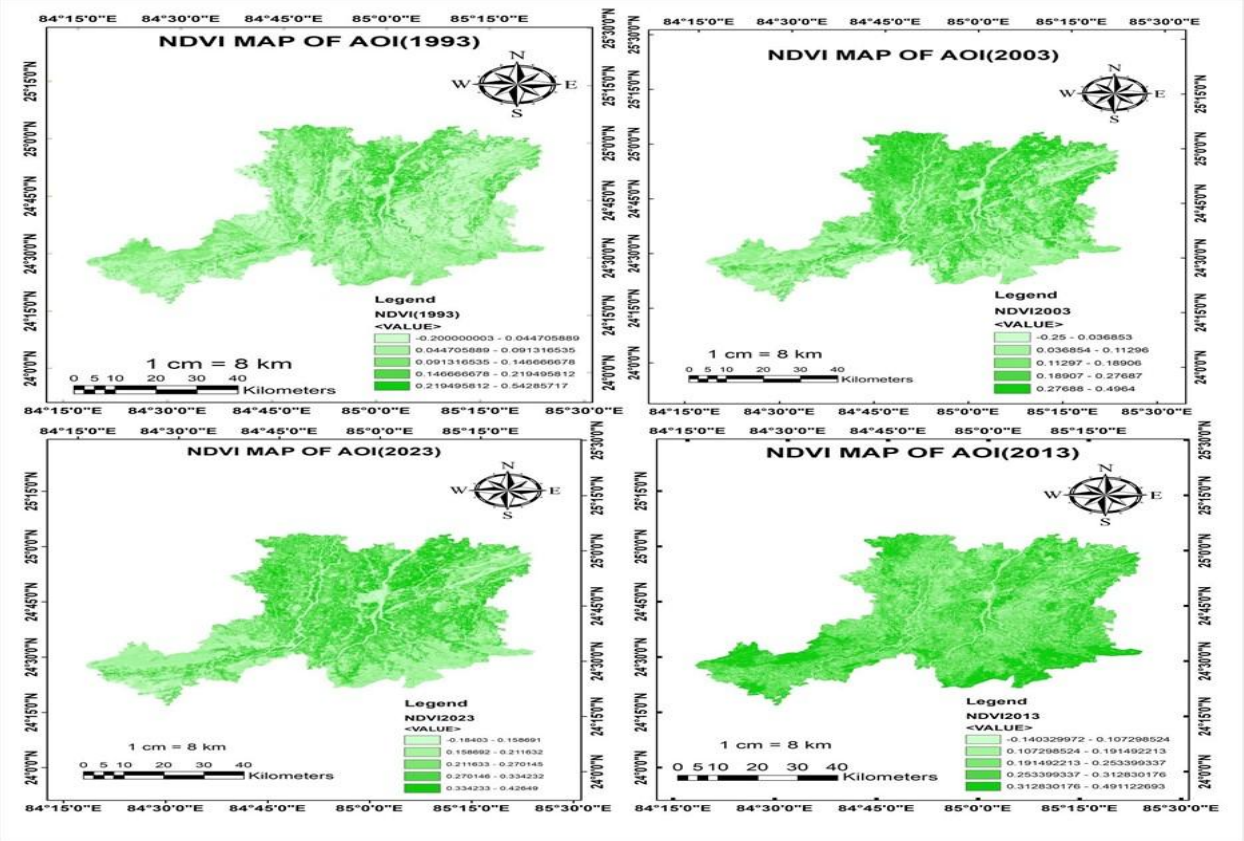

Fig. 5: *NDVI* maps of AOI in 1993, 2003, 2013 and 2023.

radiation. The alteration in surface intensity transition is observed with an increase in the albedo of the planet. Regions

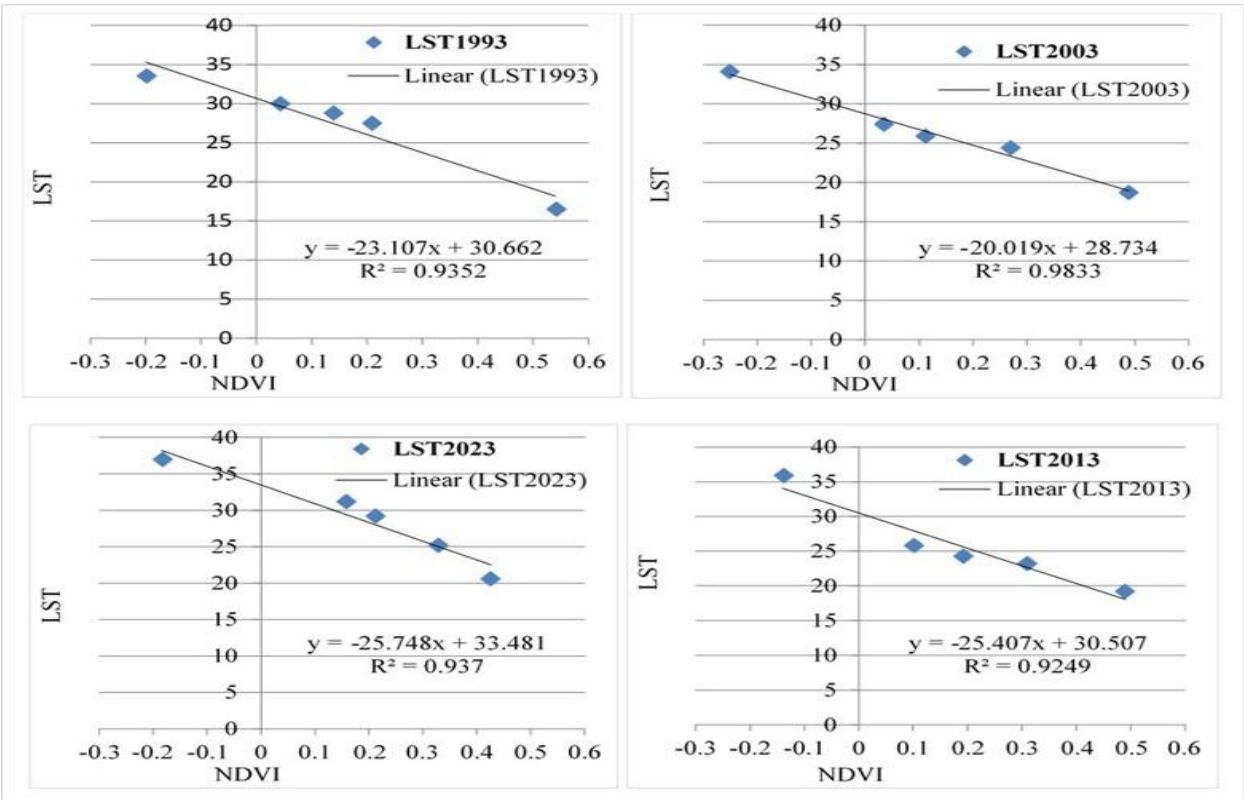

Fig. 6: *NDVI* vs. *LST* of AOI in 1993, 2003, 2013 and 2023.

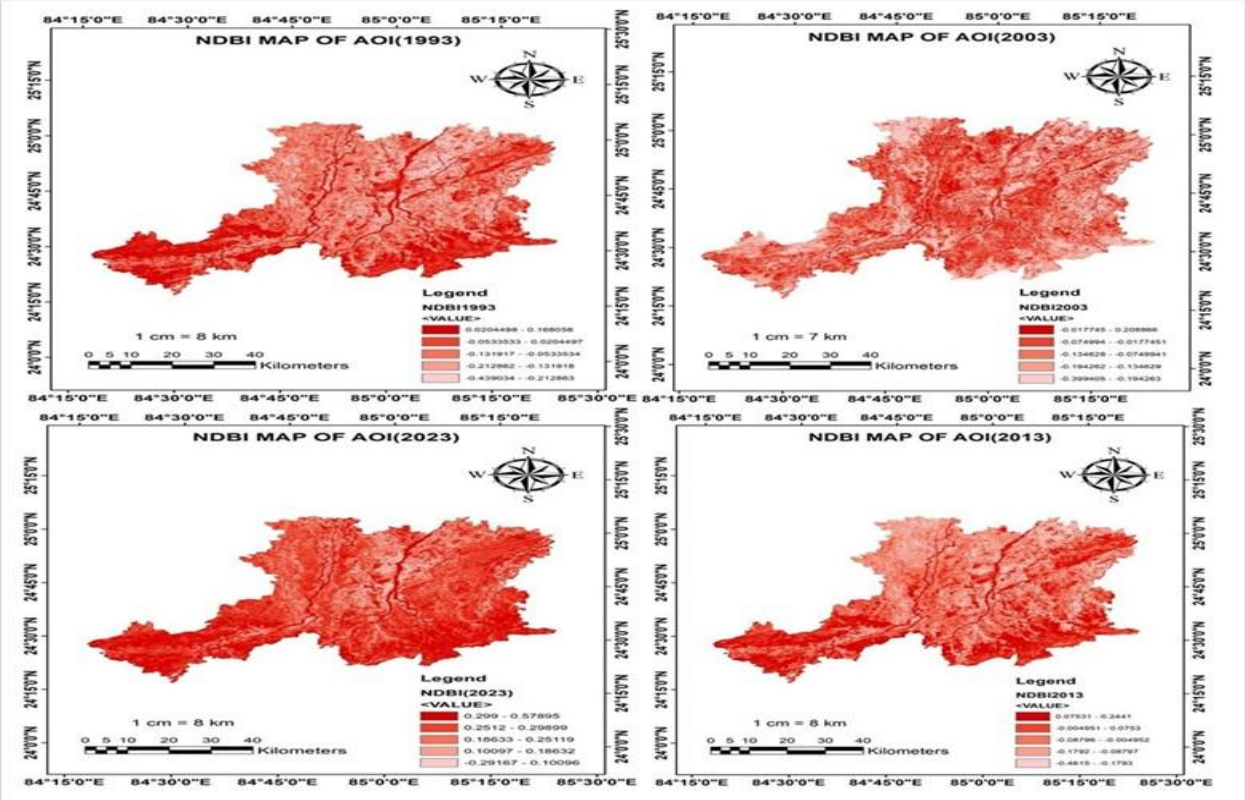

Fig. 7: *NDBI* maps of AOI in 1993, 2003, 2013 and 2023.

devoid of vegetation can experience an increase in the Earth's albedo. Typically, woodlands exhibit a low albedo due to their capacity to absorb a significant portion of the visible spectrum of light through the process of photosynthesis. This phenomenon results in a cooling effect on the surrounding environment.

The surface temperature was obtained through the use of the thermal band of the Landsat satellite. The correlation between temperature and land use was effectively discerned solely based on surface temperature data. Landsat images over the study area covering 1993, 2003, 2013, and 2023 were used to examine surface temperature. In March of 1993, during the spring season, the surface temperature was found to vary from 33.5℃ to16.5℃. In the year 2003, the highest recorded land surface temperature was 34.1 ℃, while the lowest recorded temperature was 18.7 ℃. At the micro-scale, alterations to the LULC have resulted in modifications to the surrounding environment. The rate of temperature change is increasing over the course of decades due to changes in land use and land cover, particularly in developed areas and open forested regions. In 2013, the highest recorded temperature was 35.9℃, while the baseline temperature was 19.2℃. The maximum temperature recorded in the year 2023 has risen to 37℃, owing to an increase in the base temperature to 20.6℃. Fig. 4 depicts all *LST* maps of the study area from 1993 to 2023. The maximum land surface temperature is depicted in dark red on all maps, while the lowest land surface temperature is depicted in green. With fast land-use and land-cover changes, the temporal change of land surface temperature has changed.

NDVI Changes

The *NDVI* maps were created using Satellite data of 1993, 2003, 2013, and 2023 (Fig. 5). *NDVI* values in the study region ranged from -0.20 to +0.542 in 1993 but changed in 2003 (minimum -0.25 and maximum +0.496). *NDVI* values changed from minimum -0.140 to maximum +0.4911 in 2013, and a change from minimum -0.184 to 0.426 was observed with 2023 data. Higher *NDVI* values revealed the most valuable and useful zones, such as vegetation and agriculture. In contrast to the usual, decreasing *NDVI* upsides revealed that there are fewer and fewer helpful locations and developing regions. When comparing maps from 1993 to 2023, there was a significant difference in *NDVI* values. The declining trend in *NDVI* value clearly indicates a loss of greenness from 1993 to 2023.

Correlation Between *NDVI* and *LST*

Results of *NDVI* changes discussed above reveal that reduced vegetation-cover indicates a higher value of *LST*. As a result, there seems to be a substantial negative association between surface temperature and *NDVI*, and in line with previous studies (Malik *et al.*, 2019). To demonstrate the variations in green areas, graphs between *LST* and *NDVI* are plotted for all four years (1993 to 2023). Fig. 6 indicates a diminishing trend in vegetation cover and suggests a negative link between *LST* and *NDVI*.

NDBI Changes

The *NDBI* maps were created using Landsat images from 1993, 2003, 2013, and 2023 (Fig. 7). Results from Fig. 7

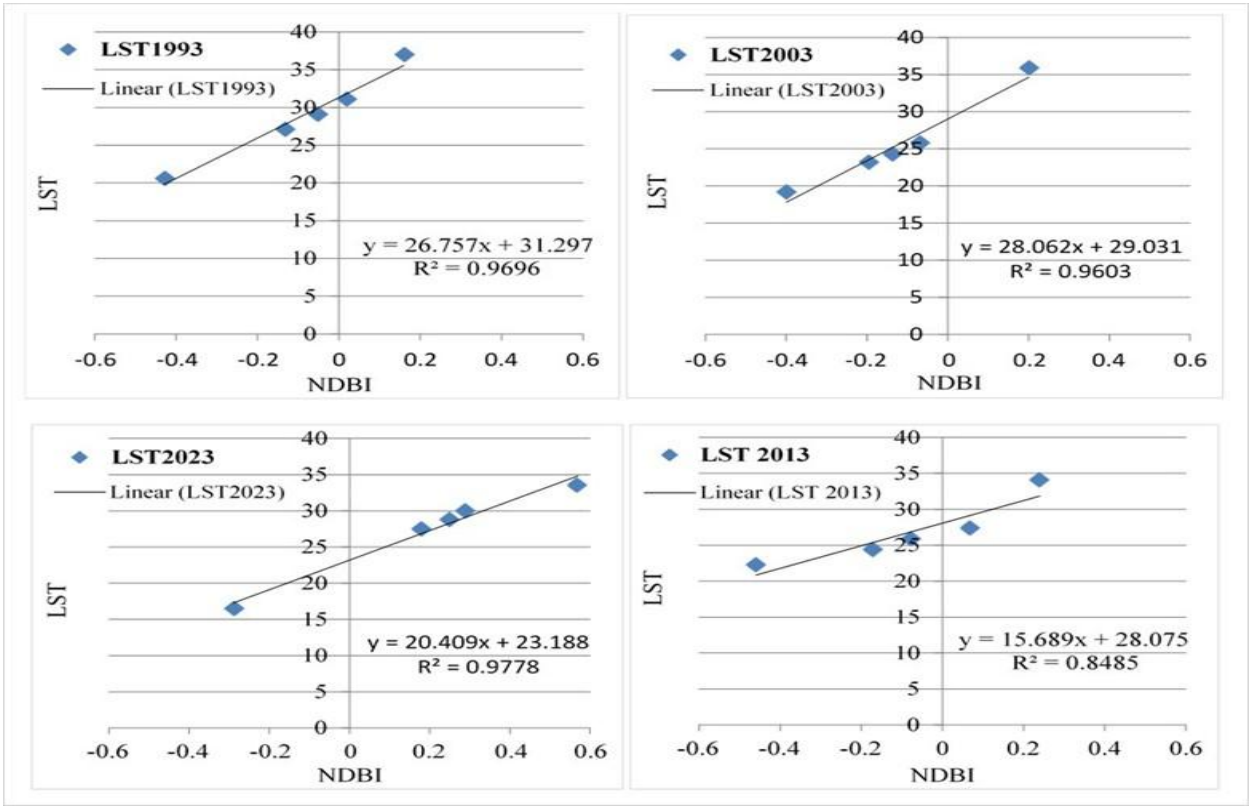

Fig. 8: *NDBI* vs. *LST* of AOI in 1993, 2003, 2013 and 2023.

indicate that *NDBI* values ranged from -0.439 to +0.168 in 1993 but changed to -0.399 to +0.20 in 2003. In 2013, *NDBI* values ranged from -0.439 to +0.244, whereas it was found to vary from 0.291 to + 0.578 in 2023, suggesting a significant shift in *NDBI* values in 2023. These results demonstrate the presence of a high-density built-up area.

Correlation Between *NDBI* and *LST*

To study the changes in built-up areas and the *LST*, graphs between *NDBI* and *LST* values are plotted for each year (Fig. 8). Results from this figure indicate a positive association between *LST* and *NDBI* (the R^2 value for the year 1993 is 0.969, 0.960 for 2003, 0.848 for 2013, and 0.9778 for 2023), and are in line with other studies (Guha *et al.*, 2021; Guha *et al.*, 2022).

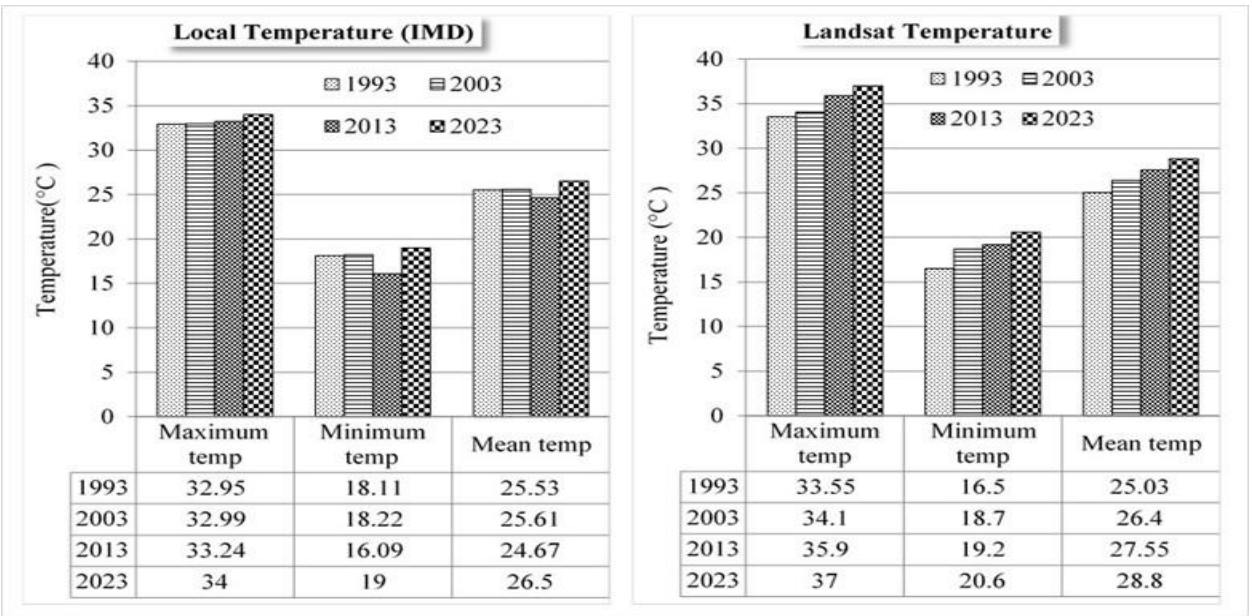

Fig. 9: Comparison of actual local temperature and computed Landsat temperature.

Comparison of Actual Local Temperature and Satellite-observed Temperature

In context to compare the results of land surface temperature data (T_{max}, T_{min}, and T_{mean}) obtained by computing the thermal band of Landsat images, local temperature data of the study area were also obtained from Indian Metrological Department, Pune (India) (Fig. 9). In general, the temperature computed from the thermal band of Landsat images was higher than the actual measured temperature as is statistically supported by an average percentage error of -5.42%. However, the actual and computed temperature exhibited a strong correlation of 0.979 with a low root mean square error of 1.98. The standard deviation in the case of T_{max}, T_{min}, and T_{mean} was 1.47, 1.46 and 1.37 respectively.

CONCLUSIONS

Time series analysis of Landsat data in terms of LULC classification and LST used in this study provides some interesting conclusions about the study area. The observed pattern of change during the timeline spanning from 1993 to 2023 primarily entails an expansion in the area of crop land and urban land with a small increase in water body coverage. The study suggests a reduction in the area of forest land and barren land due to the rise in the built-up area as well as the conversion of barren land to crop lands. Additionally, the study also suggests that the area of water bodies also experienced an increase during the same time period.

Conclusions in terms of LST values suggest an increase in land surface temperature between 1993 and 2023, which can be attributed to the expanding build-up area in a westward direction within the study area. Plots between $NDVI$ and LST, as well as $NDBI$ and LST, suggest the same trends as reported in earlier studies covering different areas.

Finally, it can be concluded that the outcomes of this study can be employed in local and town planning as well as in the management of agriculture in the near future, amidst rapid changes in the environment in the study area. While urbanisation remains an ongoing trend, it is possible to implement management strategies to regulate the increasing LST by increasing the plantations.

Acknowledgement

The authors are thankful to the National Institute of Technology Kurukshetra (India) for providing all of the resources needed for the study.

Grant Support Details

The present research did not receive any financial support.

Conflict of Interest

The authors declare that there is not any conflict of interests regarding the publication of this manuscript. In addition, the ethical issues, including plagiarism, informed consent, misconduct, data fabrication and/ or falsification, double publication and/or submission, and redundancy, has been completely observed by the authors.

Life Science Reporting

No life science threat was practiced in this research.

REFERENCES

1) Ahmad, F., Goparaju, L. and Qayum, A. (2017) 'LULC analysis of urban spaces using Markov chain predictive model at Ranchi in India', *Spatial Information Research*, 25, pp. 351–359. doi:10.1007/s41324-017-0102-x.
2) Bisht, P., Deswal, S. and Pal, M. (2023) 'Land surface temperature extraction using Landsat data over Dehradun, India: assessment of various retrieval algorithms and emissivity models', *Suranaree Journal of Science and Technology*, 30(6), pp. 010282. doi:10.55766/sujst-2023-06-e02912.
3) Boori, M.S., Voženílek, V. and Choudhary, K. (2015) 'Land use/cover disturbance due to tourism in Jeseníky Mountain, Czech Republic: a remote sensing and GIS based approach', *Egyptian Journal of Remote Sensing and Space Sciences*, 18(1), pp. 17–26. doi:10.1016/j.ejrs.2014.12.002.
4) Census (2011) *District census handbook: Gaya 2011*. Available at: https://www.census2011.co.in/census/district/88-gaya.html (Accessed: 20 May 2023).
5) Chaudhuri, G. and Mishra, N.B. (2016) 'Spatio-temporal dynamics of land cover and land surface temperature in Ganges-Brahmaputra delta: a comparative analysis between India and Bangladesh', *Applied Geography*, 68, pp. 68–83. doi:10.1016/j.apgeog.2016.01.002.
6) Conrad, C., Dech, S.W., Hafeez, M., Lamers, J.P.A. and Tischbein, B. (2013) 'Remote sensing and hydrological measurement based irrigation performance assessments in the upper Amu Darya Delta, Central Asia', *Physics and Chemistry of the Earth, Parts A/B/C*, 61–62, pp. 52–62. doi:10.1016/j.pce.2013.05.002.
7) Das, N., Mondal, P., Sutradhar, S. and Ghosh, R. (2021) 'Assessment of variation of land use/land cover and its impact on land surface temperature of Asansol subdivision', *Egyptian Journal of Remote Sensing and Space Sciences*, 24(1), pp. 131–149. doi:10.1016/j.ejrs.2020.05.001.
8) Ding, H. and Shi, W. (2013) 'Land-use/land-cover change and its influence on surface temperature: a case study in Beijing City', *International Journal of Remote Sensing*, 34(15), pp. 5503–5517. doi:10.1080/01431161.2013.792966.
9) Egorov, A.V., Roy, D.P., Zhang, H.K., Hansen, M.C. and Kommareddy, A. (2018) 'Demonstration of percent tree cover mapping using Landsat analysis ready data (ARD) and sensitivity with respect to Landsat ARD processing level', *Remote Sensing*, 10(2), p. 209. doi:10.3390/rs10020209.
10) Foody, G.M. (1992) 'On the compensation for chance agreement in image classification accuracy assessment', *Photogrammetric Engineering & Remote Sensing*, 58(10), pp. 1459–1460. Available at: https://www.asprs.org/wp-content/uploads/pers/1992journal/oct/1992_oct_1459-1460.pdf
11) Gashu, K. and GebreEgziabher, T. (2018) 'Correction to: spatiotemporal trends of urban land use/land cover and green infrastructure change in two Ethiopian cities: Bahir Dar and Hawassa', *Environmental Systems Research*, 7, p. 11. doi:10.1186/s40068-018-0114-0.
12) Gondwe, J.F., Lin, S. and Munthali, R.M. (2021) 'Analysis of land use and land cover changes in urban areas using remote sensing: case of Blantyre City', *Discrete Dynamics in Nature and Society*, 2021(1), 8011565. doi:10.1155/2021/8011565.
13) Guha, S., Govil, H., Gill, N. and Dey, A. (2021) 'A long-term seasonal analysis on the relationship between LST and NDBI using Landsat data', *Quaternary International*, 575–576, pp. 249–258. doi:10.1016/j.quaint.2020.06.041.
14) Guha, S., Govil, H., Taloor, A.K., Gill, N. and Dey, A. (2022) 'Land surface temperature and spectral indices: A seasonal study of Raipur City', *Geodesy and Geodynamics*, 13(1), pp. 72–82. doi:10.1016/j.geog.2021.05.002.
15) Hashim, A.M., Elkelish, A., Alhaithloul, H.A., El-hadidy, S.M. and Farouk, H. (2020) 'Environmental monitoring and prediction of land use and land cover spatio-temporal changes: a case study from El-Omayed Biosphere Reserve, Egypt', *Environmental Science and Pollution Research*, 27, pp. 42881–42897. doi:10.1007/s11356-020-10208-1.
16) Hassan, Z., Shabbir, R., Ahmad, S.S., Malik, A.H., Aziz, N., Butt, A. and Erum, S. (2016) 'Dynamics of land use and land cover change (LULCC) using geospatial techniques: a case study of Islamabad Pakistan', *SpringerPlus*, 5, p. 812. doi:10.1186/s40064-016-2414-z.
17) Kausarian, H., Redyafry, L., Sumantyo, J.T.S., Suryadi, A. and Lubis, M.Z. (2023) 'Structural analysis of the central Sumatra Basin using

geological mapping and Landsat 8 oli/tirsC2 L1 data', *EVERGREEN Joint Journal of Novel Carbon Resource Sciences & Green Asia Strategy*, 10(2), pp. 792–804. doi:10.5109/6792830.
18) Kawo, N.S., Hordofa, A.T. and Karuppannan, S. (2021) 'Performance evaluation of GPM-IMERG early and late rainfall estimates over Lake Hawassa catchment, Rift Valley Basin, Ethiopia', *Arabian Journal of Geosciences*, 14, p. 256. doi:10.1007/s12517-021-06599-1.
19) Koko, A.F., Wu, Y., Abubakar, G.A., Alabsi, A.A.N., Hamed, R. and Bello, M. (2021) 'Thirty years of land use/land cover changes and their impact on urban climate: a study of Kano Metropolis, Nigeria', *Land*, 10(11), p. 1106. doi:10.3390/land10111106.
20) Laosuwan, T. and Sangpradit, S. (2012) 'Urban heat island monitoring and analysis by using integration of satellite data and knowledge based method', *International Journal of Development and Sustainability*, 1(2), pp. 99–110. Available at: https://isdsnet.com/ijds-v1n2-4.pdf
21) Lunetta, R.S., Ioames, J., Knight, J., Congalton, R.G. and Mace, T.H. (2001) 'An assessment of reference data variability using a virtual field reference database', *Photogrammetric Engineering & Remote Sensing*, 63(6), pp. 707–715. Available at: https://www.asprs.org/wp-content/uploads/pers/2001journal/june/2001_jun_707-715.pdf
22) Ma, Z. and Redmond, R.L. (1995) 'Tau coefficients for accuracy assessment of classification of remote sensing data', *Photogrammetric Engineering & Remote Sensing*, 61(4), pp. 435–439. Available at: https://www.asprs.org/wp-content/uploads/pers/1995journal/apr/1995_apr_435-439.pdf
23) Malik, M.S., Shukla, J.P. and Mishra, S. (2019) 'Relationship of LST, NDBI and NDVI using Landsat-8 data in Kandaihimmat Watershed, Hoshangabad, India', *Indian Journal of Geo-Marine Science*, 48(1), pp. 25–31. Available at: https://core.ac.uk/download/pdf/297996963.pdf
24) Moldakhanova, N., Alimkulov, S. and Smagulov, Z. (2023) 'Analysis of changes in the ecological space of the Ili river delta (due to reduced flow of the Ili River)', *EVERGREEN Joint Journal of Novel Carbon Resource Sciences & Green Asia Strategy*, 10(1), pp. 29–35. doi:10.5109/6781031.
25) Pal, S. and Ziaul, S.K. (2017) 'Detection of land use and land cover change and land surface temperature in English Bazar urban centre', *Egyptian Journal of Remote Sensing and Space Science*, 20, pp. 125–145. doi:10.1016/j.ejrs.2016.11.003.
26) Pranoto, B., Adilla, I., Soekarno, H., Supriatna, N.K., Adrian, L., Efiyanti, D., Indrawan, A., Hesty, N.W. and Fithri, S.R. (2023) 'Using satellite data of palm oil area for potential utilization in calculating palm oil trunk waste as cofiring fuel biomass', *EVERGREEN Joint Journal of Novel Carbon Resource Sciences & Green Asia Strategy*, 10(3), pp. 1784–1791. doi:10.5109/7151728.
27) Reis, S. (2008) 'Analyzing land use/land cover changes using remote sensing and GIS in Rize, North-East Turkey', *Sensors*, 8(10), pp. 6188–6202. doi:10.3390/s8106188.
28) Robertson, L.D. and King, D.J. (2011) 'Comparison of pixel- and object-based classification in land cover change mapping', *International Journal of Remote Sensing*, 32(6), pp. 1505–1529. doi:10.1080/01431160903571791.
29) Saharan, S., Deswal, S. and Pal, M. (2024) 'Air quality mapping and urban planning for sustainable urban ecology: a case study of Chandigarh, India', *Ecological Questions*, 35(2), pp. 1–15. doi:10.12775/EQ.2024.020.
30) Shekhar, D. and Godihal, J. (2023) 'Exploring the mechanical and microstructural characteristics of recycled concrete hollow blocks: transforming waste into valuable resources', *EVERGREEN Joint Journal of Novel Carbon Resource Sciences & Green Asia Strategy*, 10(4), pp. 2195–2206. doi:10.5109/7160894.
31) Townshend, J.R.G. and Justice, C.O. (1986) 'Analysis of the dynamics of African vegetation using the normalized difference vegetation index', *International Journal of Remote Sensing*, 7(11), pp. 1435–1445. doi:10.1080/01431168608948946.
32) Wang, B., Choi, J., Choi, S., Lee, S., Wu, P. and Gao, Y. (2017) 'Image fusion-based land cover change detection using multi-temporal high-resolution satellite images', *Remote Sensing*, 9(8), p. 804. doi:10.3390/rs9080804.
33) Yermekbayev, B.K., Dzhangarasheva, N.V. and Rakhimzhanova, G.M. (2023) 'Overview of grazing as a land use system in Kazakhstan', *EVERGREEN Joint Journal of Novel Carbon Resource Sciences & Green Asia Strategy*, 10(2), pp. 658–666. doi:10.5109/6792812.
34) Yussupov, A. and Suleimenova, R.Z. (2023) 'Use of remote sensing data for environmental monitoring of desertification', *EVERGREEN Joint Journal of Novel Carbon Resource Sciences & Green Asia Strategy*, 10(1), pp. 300–307. Available at: https://www.tj.kyushu-u.ac.jp/evergreen/contents/EG2023-10_1_content/pdf/p300-307.pdf
35) Zha, Y., Gao, J. and Ni, S. (2003) 'Use of normalized difference built-up index in automatically mapping urban areas from TM imagery', *International Journal of Remote Sensing*, 24(3), pp. 583–594. doi:10.1080/01431160304987.
36) Zhou, Q., Robson, M. and Pilesjo, P. (1998) 'On the ground estimation of vegetation cover in Australian rangelands', *International Journal of Remote Sensing*, 19(9), pp. 1815–1820. doi:10.1080/014311698215261.